U.S. Department of Energy
Golden Field Office

DE-EE0000574

AccuStrata, Inc.
387 Technology Drive, Suite 1100
University of Maryland, College Park, MD 20742
(301) 314 - 2116

Project Title:

Real time intelligent process control system for thin film solar cell manufacturing

Principal Investigator:
George Atanasoff, PhD

Executive Summary

This project addresses the problem of lower solar conversion efficiency and waste in the typical solar cell manufacturing process. The work from the proposed development will lead toward developing a system which should be able to increase solar panel conversion efficiency by an additional 12-15% resulting in lower cost panels, increased solar technology adoption, reduced carbon emissions and reduced dependency on foreign oil.

All solar cell manufacturing processes today suffer from manufacturing inefficiencies that currently lead to lower product quality and lower conversion efficiency, increased product cost and greater material and energy consumption. This results in slower solar energy adoption and extends the time solar cells will reach grid parity with traditional energy sources. The thin film solar panel manufacturers struggle on a daily basis with the problem of thin film thickness non-uniformity and other parameters variances over the deposited substrates, which significantly degrade their manufacturing yield and quality. Optical monitoring of the thin films during the process of the film deposition is widely perceived as a necessary step towards resolving the non-uniformity and non-homogeneity problem.

In order to enable the development of an optical control system for solar cell manufacturing, a new type of low cost optical sensor is needed, able to acquire local information about the panel under deposition and measure its local characteristics, including the light scattering in very close proximity to the surface of the film. This information cannot be obtained by monitoring from outside the deposition chamber (as traditional monitoring systems do) due to the significant signal attenuation and loss of its scattering component before the reflected beam reaches the detector. In addition, it would be too costly to install traditional external in-situ monitoring systems to perform any real-time monitoring over large solar panels, since it would require significant equipment refurbishing needed for installation of multiple separate ellipsometric systems, and development of customized software to control all of them simultaneously.

The proposed optical monitoring system comprises AccuStrata's fiber optics sensors installed inside the thin film deposition equipment, a hardware module of different components (beyond the scope of this project) and our software program with iterative predicting capability able to control material bandgap and surface roughness as films are deposited. Our miniature fiber optics monitoring sensors are installed inside the vacuum chamber compartments in very close proximity where the independent layers are deposited (an option patented by us in 2003). The optical monitoring system measures two of the most important parameters of the photovoltaic thin films during deposition on a moving solar panel - material bandgap and surface roughness. In this program each sensor array consists of two fiber optics sensors monitoring two independent areas of the panel under deposition. Based on the monitored parameters and their change in time and from position to position on the panel, the system is able to provide to the equipment operator immediate information about the thin films as they are deposited. This DoE Supply Chain program is considered the first step towards the development of intelligent optical control system capable of dynamically adjusting the manufacturing process "on-the-fly" in order to achieve better performance.

The proposed system will improve the thin film solar cell manufacturing by improving the quality of the individual solar cells and will allow for the manufacturing of more consistent and uniform products resulting in higher solar conversion efficiency and manufacturing yield. It will have a significant impact on the multibillion-dollar thin film solar market.

We estimate that the financial impact of these improvements if adopted by only 10% of the industry ($7.7 Billion) would result in about $1.5 Billion in savings by 2015 (at the assumed 20% improvement). This can be achieved by optimizing the manufactured product and process in real time without changing the manufacturing technology.

Project Activity Summary

Figure 1 illustrates the scope of this DoE Supply Chain project, which is marked in light green color. This project covered the development of the fiber optics sensors and the supporting fiber optics assembly, the installation of the sensors in the deposition equipment of our industrial partner. This included the design of the needed fiber optic feedthrough for the chamber walls, the validation of the installed systems in real manufacturing and their operation. A significant part of the project was the development of an algorithm and software for monitoring and calculation of the film material bandgap and its surface roughness. The last two parameters play a critical role in the final efficiency of the solar panels and currently are not monitored for each panel, leaving a lot of room for improvement.

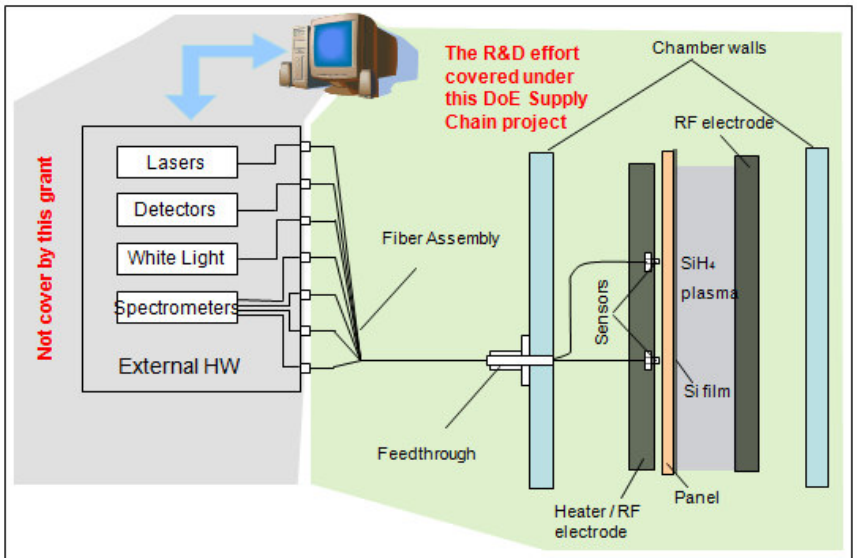

Figure 1. This DoE Supply Chain project covered the development, installation, validation and operation of the fiber optics sensors, the fiber assemblies and the vacuum feed-throughs. It also covered the development of the project specific software features – the film band-gap and surface roughness. The external hardware module and some other software features not covered by this project.

The hardware module, including the light sources and the light detectors and the data acquisition software that operates the hardware module are not in the scope of this DoE project. Also excluded from this project is the main parameter calculation algorithm and software, including the software features that calculate the film optical constants n&k and the film thickness during the deposition of the films.

Accomplishments vs. Objectives

Develop and install a prototype real-time optical control system for measuring material band-gap and surface roughness on moving thin film solar panels in a manufacturing line.

This objective is achieved by:

1) Develop an alpha-prototype system to monitor thin film panel deposition. The system will be able to detect surface roughness and material bandgap and their uniformity over the panel area in real time on a moving panel. This objective is achieved 100%.
2) Develop a software program able to measure in real time the optical scattering from the panel surface and calculate surface roughness. This objective is achieved 100%.
3) Develop a software program able to measure in real time the material bandgap of the deposited photovoltaic films. This objective is achieved 100%.
4) Validate the system in real thin film solar panel deposition process. This objective is achieved 100%.

The expected outcome of this project is a prototype of optical monitoring system with application to manufacturing of higher efficiency thin film solar panels

Task 1: Build customized optical sensors and assemble 2 identical 2-sensor arrays monitoring subsystem

Expected Outcome/Milestone: Fiber optics sensors able to meet the requirements

Approach 1


Figure 2. The first generation of fiber optic sensor used 7 fibers at normal incidence as well as at 15º, 25º and 35º.

Our initial design for an optical sensor used an aluminum sensor head shown in Figure 2 to support 7 600 μm Al-clad fibers able to operate at high temperatures of up to 320°C. The fibers are inserted into the sensor head and fixed by setscrews. This sensor design made use of 4 cool-white LEDs each coupled into its 600 μm fiber (the hardware module with all light sources and detectors is not covered by this project). The light from each LED shines through the optical sensors at different incident angle (0, 15, 25 and 35 degrees). A 5th fiber collects the reflected light from the panel and brings it back to the spectrometer. The LEDs are controlled and time sequenced so that only one LED would be active at a time to ensure that the separate light sources did not interfere with one another. In addition to the spectrometer and the four LEDs there are also two other fibers, one that sends an 850nm laser beam at the substrate (#6) and another (#7) that receives the reflectance of the laser light from the panel surface and brings it back to a detector.

Approach 1 – Problems Encountered

After building, testing and installing the sensor head from Figure 2 we found a few issues of concern with this design. The first issue was that the light from the laser source from the 6th fiber creates a noise to the spectrometer for white light and frequently saturates the CCD detector of the spectrometer. The second issue was related to the white light from the LEDs, which created some noise for the stand alone detector, designed to collect the reflected 850 nm laser light. The installation of a variety of band-pass filters and fiber attenuators did not resolve the problems entirely and resulted in additional cost. In addition we were not able to collect sufficient reflected signal at some of the angles of incidence.

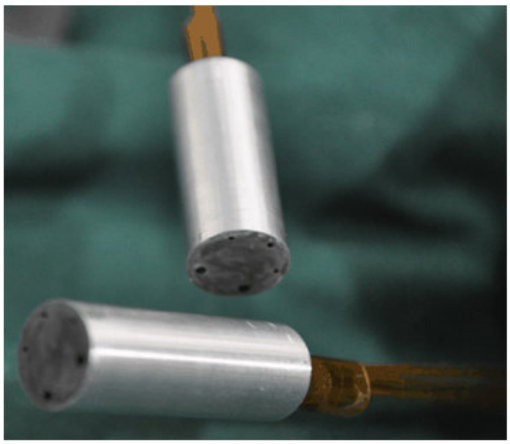
Figure 3. The second generation of sensor used a bundle of 200 μm fibers.

Approach 2

In order to address the problems discussed in the previous section we have developed a new sensor head shown in Figure 3. This new sensor no longer used the 600um aluminum clad fibers; instead it used bundles of multiple 200um fibers. This design solved the issue of cross contamination from the laser light going into the spectrometer by positioning the LED and spectrometer fibers as far as possible from the laser and detector fibers on the sensor face.

Approach 2 – Problems Encountered

The major problem with this new sensor was the lack of signal strength which was actually made worse by the use of 200 μm fiber bundles instead of the solitary 600 μm aluminum clad fiber. Because the lack of signal strength using this new sensor was a

critical problem that prevented any real data collection it was never installed in an active deposition chamber and instead we immediately created a third design. Another concern was the use of polyimide-coated fibers (versus Al-clad fibers which would be too expensive), which were not able to withstand the high temperature. After testing the polyimide fibers for several days inside the deposition chamber, we have decided to abandon this design for concerns about outgasing.

Approach 3

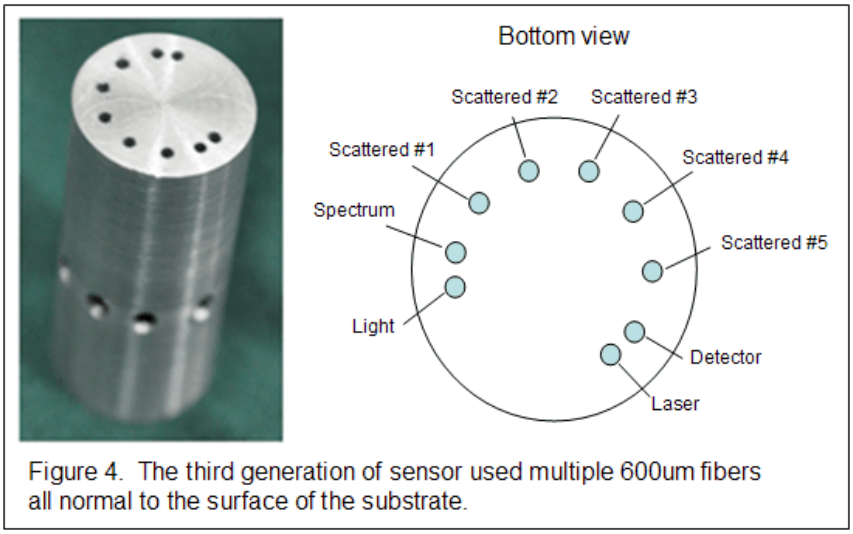

Figure 4. The third generation of sensor used multiple 600um fibers all normal to the surface of the substrate.

The third and last sensor developed under the project, shown in Figure 4, provided for having the laser and spectrometer fibers far enough away from each other to avoid crosstalk. This design exchanged the angled fibers for 600 µm Al-clad fibers at normal incidence. This sensor was able to measure the reflected light which allowed for the calculation of the surface roughness of the material. Exchanging the angled fibers also helped us reduce costs associated with production of the sensor heads and in the overall cost of the system since it is more costly to bore a square hole than a round hole.

In the third sensor we also made one major change to the hardware module that affected the sensor heads. We went from sequentially illuminating the substrate with 4 white light LEDs to using one white light source (halogen light source). Since the white light source could not be turned on and off fast enough, we redesigned the system in a way that there was one illuminating fiber and several reflectance receptive fibers. One channel was used to measure the spectral data and the second channel used light from a fiber, which was positioned further away from the source, in order to measure the scattered reflectance needed for the calculation of the surface roughness. This new approach allowed us to collect all the data continuously instead of sequentially, as was previously the case.

Approach 3 – Problems Encountered

No major problems were found using the third generation of sensor head, however, we did find some find some methods that allowed us to simplify our design and make it more streamlined and less costly to manufacture.

Solutions

In order to make our sensor head as streamlined and economical as possible we made a few changes and built them in to our final design as shown in Figure 5. The

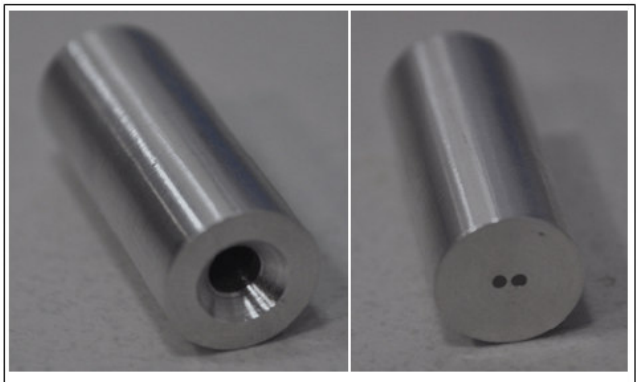

Figure 5. The final and current version of the sensor head as seen from the back (left) and front (right)

first of these was based off the fact that we achieved acceptable results using our standard light source and spectrometer to measure the reflectance at variable wavelengths. We extracted the time-domain data for each wavelength from the broadband spectral scans, from 400 nm to 920 nm and demonstrated that the results are acceptable without the need for the time-domain 850 nm laser source and detector. The accuracy of this approach was lower, but the iterative prediction capability, built into our calculation algorithm allowed us to calculate the needed parameter at one wavelength and validate it at multiple other wavelengths with additional correction when needed. This allowed us to remove the laser and the standing alone detector from our system, eliminate the noise problem and reduce the number of fibers needed in the sensor head without compromising the accuracy of calculations.

The second solution was that once the diffuse reflectance of the panel with the pre-deposited TCO layer is measured and characterized, the diffuse scattering (measured from the back side of the panel) is not changing during the deposition of the p- and i-layers and remains constant until the entire panel is deposited. We therefore only needed the sensor as shown in Figure 4 for the p-layer deposition compartment, where the panel with TCO first enters the deposition equipment. For the i-layer compartment, we simplified the sensor design and used a simpler sensor with only 2 fibers.

As a result of this work this task was completed 100%. The milestone has been achieved

Task 2: Install the optical sensors inside existing manufacturing line of a solar panel manufacturer

Expected Outcome/Milestone: Installed optical monitoring system in a real manufacturing line for thin film solar panels

Approach

We had to determine how to fix the sensor heads in place inside the deposition chamber, how to feed the fiber optic cables into the chamber and how to perform the optical monitoring without contaminating the sensor heads and the fiber facets.

The installation of two fiber optics monitoring systems at the manufacturing facility of our industrial partner is shown in Figure 6. One of the monitoring systems is installed in the chamber compartment for deposition of the p-Si thin film (shown on the right side) and the second one in the compartment for the deposition of the i-Si absorber layer (shown on the left side)

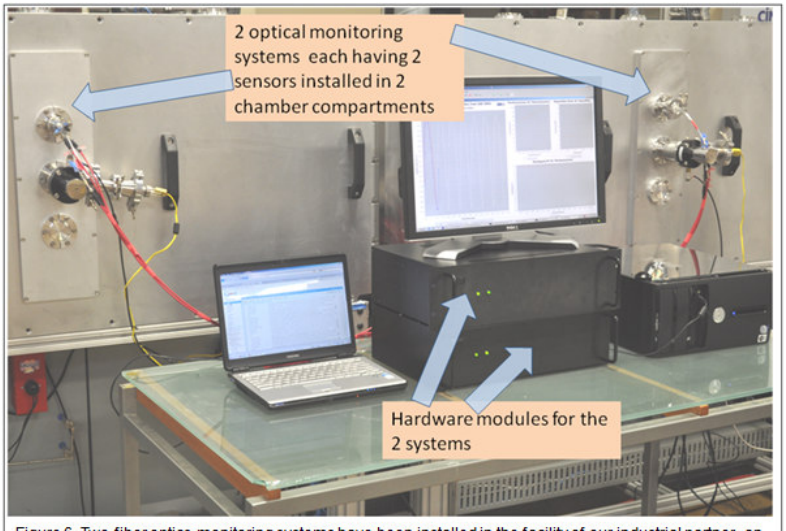

Figure 6. Two fiber optics monitoring systems have been installed in the facility of our industrial partner- an amorphous silicon thin film solar panel manufacturer. The monitoring system installed on the right monitors the p-Si thin film layer and system on the left monitors the i-Si thin film layer.

Problems Encountered

- The first problem is to find fibers that would be able to withstand temperatures of up to 300°C while still being flexible enough to be installed in the tight confines of the chamber.

Solution: We researched a variety of fibers and materials used in making fibers and eventually found a solution in aluminum clad silica fibers. These fibers are able to safely withstand heating up to 300°C but still retain the flexibility needed inside the chamber to reach from the fiber optic feed through to the sensor head itself. The bending radius of the Al-clad 600 µm silica fibers allows them to be bent to about 12-15 mm without compromising the fiber optical loss. However, larger bending is also possible, down to a radius of 3-4 mm (even though the fiber exercises optical loss) without breaking or damaging the fiber. These fibers gave us the needed flexibility to operate in the confined space behind the optical sensor.

- The next problem is the fiber preparation, including the fibers inside and outside the deposition equipment, the connectors and fiber jacketing.

  Solution: We purchased fiber preparation equipment, including a fiber cleaver, fiber stripper and fiber polisher. This equipment was purchased with company's private funds. We also trained our engineers to be able to cleave and polish large-core Al-clad fibers. We accumulated significant experience and skills in fiber polishing, fiber coupling to light sources and connector assembly using SMA fiber connectors.

- The third problem is getting the fibers through the vacuum chamber walls of the chamber while still being able to maintain the vacuum inside the chamber. This issue was made more difficult by the fact that the solar panel manufacturer did not want any type of epoxy within the chamber itself because of possible issues with the epoxy out-gassing at high temperatures.

  Solution: We developed different methods over time as the physical shape of our sensor heads kept changing. We solved the problems of getting the fiber optic cables through a tightly drilled out feed-through flange on the wall of all the chambers. After running the fibers through the faceplate, as shown in Figure 6, we then used a vacuum sealing epoxy on the outer wall of the chamber as shown in Figure 7, where there was no possibility of high heat or out gassing, to reseal the chamber and keep it under vacuum. This simplified solution was used in our prototype development. However, throughout the program we developed a more advanced solution using removable vacuum-sealed metal shaft with fibers going through it. This solution allows us to dismantle the feed-through and reinstall the sensors without the need of changing the fibers going to the sensor head. For proprietary reasons we are not displaying the solution here.

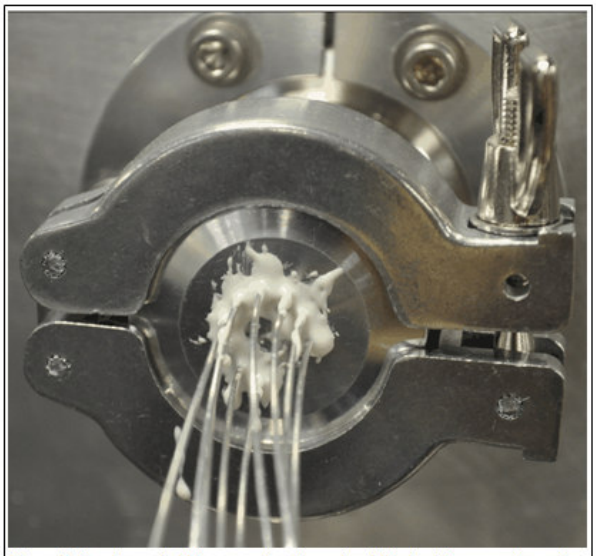

Figure 7. Aluminum clad fibers running through a drilled out flange on the wall of the chamber that have been sealed in placed to maintain vacuum.

- Finally, we faced the problem of contamination of the sensors during deposition.

  Solution: The solution to avoid the sensors contamination during the deposition process is found in the monitoring from the back-side of the glass panel. The team has a significant experience and know how in this approach and we successfully modified our monitoring and calculation algorithm in order to allow this to be a feasible solution.

As a result Task 2 has been completed 100%. The milestone has been achieved

Task 3: Develop software program for monitoring spectroscopic reflectance (specular and diffuse) in real time in both time and spectral domains and calculation of surface roughness and material bandgap

Expected Outcome/Milestone: A software program able to perform the described functions

Subtask 3.1: Develop software program for monitoring reflectance (specular and diffuse) in real time in both time and spectral domains and calculate surface roughness

Our approach to determine surface roughness by optical measurements is to calculate the film haze by measuring scattered (diffuse) light at various angles of incidence[1], as well as the specular reflected light at normal incidence. Typically haze is measured by using an integrated sphere and is defined as the ratio between the diffuse reflectance and the total reflectance: - an integral parameter over the entire spectral range and over all angles of incidence. More precise definition takes into account the dependence of haze on the incident angle and wavelength.

Two optical measurements are needed to determine optical haze $H(\theta,\lambda)$ of the TCO layer and derive the surface roughness using the scattering theory: 1) diffused (scattered) light from the film $R_{diffuse}(\theta,\lambda)$ and 2) directed (specular) reflected light $R_{specular}(\theta,\lambda)$ across the wavelength range of about 400-1000nm:

$$H(\theta,\lambda) = \frac{R_{diffuse}(\theta,\lambda)}{R_{diffuse}(\theta,\lambda) + R_{specular}(\theta,\lambda)}$$

We designed a sensor that could measure scattered light at various angles θ simultaneously, and at normal incidence (θ =0). This sensor design is described in Task 1 of this report (see Figure 2 and Figure 4).

The fact that we are measuring the reflectance at a discrete angle or angles (rather than at all angles of incidence) is accounted for by adding a calibration function C, which needs to be determined experimentally. In case of isotropic scattering, as is roughly the case with the TCO layer on glass panel, one can safely assume that C is a linear function. Haze is then calculated by the scattered reflected light collected at one angle θ_i and the specular reflected light at normal incidence, and then verified by the measurements made at the other angles.

The surface roughness can be determined by the following expression[2], derived from the scattering theory:

$$H(\lambda) = 1 - \exp\left[-\left(\frac{4\pi\delta_{RMS}C}{\lambda}\right)^2\right]$$

where δ_{rms} is the root-mean square of the surface roughness. In order to utilize this relationship we needed to measure several reference standards using Atomic Force Microscopy (AFM), to

[1] Typically haze is defined as an integral parameter over the entire spectral range and over all angles of incidence and is measured using integrated sphere. More precise definition takes into account the dependence of haze on the incident angle and wavelength. In our case measuring the diffuse reflectance at any discrete angle (rather than at all angles of incidence) is accounted by adding a calibration function C, determined experimentally. This assumption could be justified in the case of isotropic scattering, as is roughly the case with the TCO layer on glass panel.

2 J.Krc et al., Thin Solid Films, 426 (2003) 296-304;

determine surface roughness via direct measurement, and to then relate this surface roughness to the scattered light measured with the fiber optic sensor.

Multiple sample surfaces were used for the measurements of surface roughness and scattered light. These samples were collected from different batches of TCO and different manufacturers, namely Asahi Corporation and Pilkington Glass. The samples specular and diffuse reflectance were measured in a bench-top setup using our optical sensor shown in Figure 2 and Figure 4, and also measured by Atomic Force Microscopy (AFM) at the Chemical Engineering Department of the University of Maryland. From the measured data we defined a linear relationship between the surface roughness and scattering as shown in Figure 8.

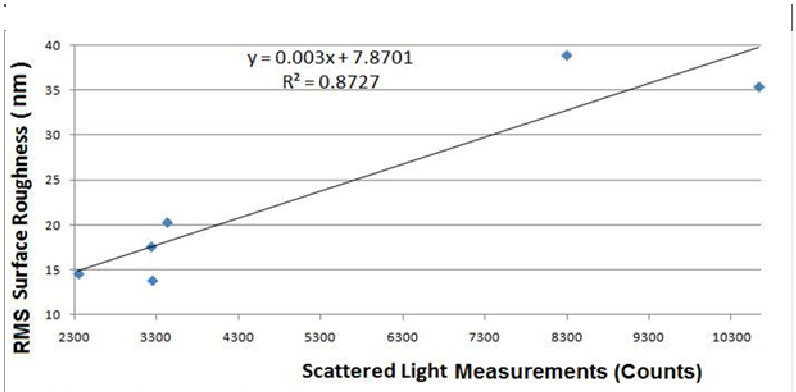

Figure 8. Linear relationship between surface roughness and scattered light measurements for 6 reference samples was found with AFM surface analysis and optical monitoring. The in situ scattering measurement was in the manufacturing environment.

Other samples were measured *in situ* inside the deposition chamber at the manufacturer's facility after the panel enters the deposition chamber immediately before the deposition of the p-layer. These panels with the deposited TCO layer were manufactured by Asahi Corporation. The thickness of the TCO was about 596 nm. We measured an average of ~10,000 spectrometer counts of scattered light at the wavelength of 385 nm. Note, that in order to simplify the measurement procedure we do not reference the scattered light (which would be too difficult to do inside the deposition chamber), and prefer to fit the measurement in the units of spectrometer's detector counts.

By the observed scattering signal for the panels inside the deposition chamber we predicted a root-mean-square (RMS) surface roughness of 38.6 nm. We then measured the same samples cut from the glass panel using AFM and determined the actual RMS surface roughness to be 32.4nm. Our resultant percent error was below ~20%.

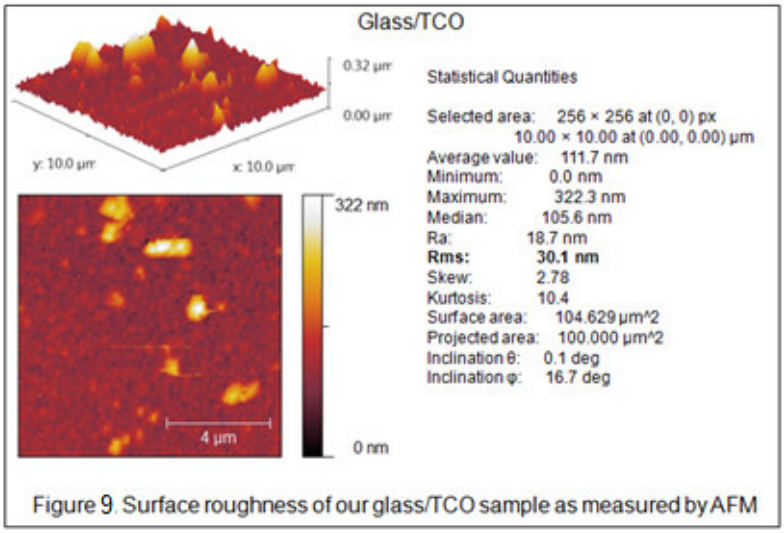

Figure 9. Surface roughness of our glass/TCO sample as measured by AFM

The AFM images were measured with Digital Instruments (Veeco) Multimode AFM with Nanoscope III controller10 micron scanner and Nanoscope Version 5.3 software. The image analysis was performed with the software Gwyddion. An example of the AFM image is shown in Figure 9 and all samples were subjected to the same analysis.

Problems Encountered

1. In practice, the amount of scattered light is much smaller compared to the amount of specular reflected light that we measured at normal incidence. This is a direct result of the characteristics of our optical sensor and the physical specimen that we wish to characterize. The TCO thin film's specular reflected light remains mostly focused in a relatively small area, thus having higher flux at the face of the specular reflectance collection fiber. The scattered light, on the other hand, is reflected at a much broader special angle, thus resulting in a very small flux being collected at the face of the scattered light collection fibers.

   Solution: Throughout the years and during the duration of this project we have been in contact with many thin film solar manufacturers both in USA and abroad. These communications have provided us a wealth of knowledge about what information is most important for manufacturing as well as what similarities exist across manufacturing methods. All amorphous silicon thin film solar panel manufacturers that are using superstrate process begin the manufacturing process with glass that has already been pre-deposited with a TCO layer. Most manufacturers purchase the panels with the TCO from outside vendors. They typically do not have any control of the roughness of the TCO surface and the light confinement coefficient that is critical for the panel efficiency. Therefore characterization of the TCO during film deposition is not needed. Another important finding is that these manufacturers frequently find variation of performance between different batches of the Glass/TCO panels that they purchase, thus making the characterization of the TCO film a necessary and welcomed step by the thin film manufacturers. From these communications we came to realize that there is great value in a system that can quickly and accurately measure scattering and calculate surface roughness of the glass/TCO surface *before* undergoing deposition. Furthermore, a map of the light scattering properties over the surface of the panel is even more appreciated, because it can show on what areas on the panel the light confinement is not sufficient. The reduced light confinement can be compensated later during deposition by increasing the thickness of the absorber at the areas of scattering deficiency.

   Therefore, the solution, which we have started developing during this DoE Supply Chain project becomes even more important for the practical needs of thin film solar manufacturers.

2. Another problem (more an observation than a problem) we have encountered is that once the deposition process of the p-, i- and n-Si layers is started the scattering properties of the panel do not change significantly. This is especially true when the optical monitoring occurs from the backside of the panel. The optical monitoring beam from the backside of the panel always sees the same scattering TCO layer and any additional scattering added by the subsequent a—Si layers is negligible. This fact allowed us to reduce the amount of work we had to do.

   Solution: This practically eases our task, since monitoring of optical scattering is needed only for the TCO layer and not for the other layers. This allows us to simplify the design of our optical sensors installed inside the deposition compartment for the i- and n-Si layers, since only the specular reflectance has to be measured. As a result we ended with the design of the sensor as shown in Figure 5. Therefore, the sensor design for the deposition chamber, where the panel enters the p-Si layer is chosen to be as shown in Figure 2 or Figure 4, while the sensors needed for the other layers are much simpler and are shown in Figure 5. This also simplifies and reduces the cost of the hardware module, since only one light source and one spectrometer is needed for each hardware module in order to monitor all the layers after the initial p-layer, where the TCO characterization takes place.

Subtask 3.2 Develop a software program for monitoring spectroscopic reflectance (specular and diffuse) in real time in the time and spectral domains and calculate the material's bandgap

Approach 1:

We used a laser (850nm) and a stand-alone Si detector. As the film grows, the reflectance at 850 nm goes through typical maximum and minimum oscillations because of the interference between incident and reflected light.

The optical thickness of the film added (attained) during the time for which the reflectance changed from one extrema to the next is equal to one quarter-wave at 850 nm or 212.5 nm. Since the refractive index of the amorphous silicon film at 850 nm is very high, typically about 3.5 to 4.0, the physical thickness gained between two extrema is~ 212.5/4.0=53.1 nm. Therefore, for each ~53 nm of physical thickness we observe an extrema in the reflectance function at 850 nm.

Please note that if we change the monitoring wavelength to, for example, 640 nm we will see similar extrema happening at each 640/4/4=40 nm). However, the wavelength 850 nm is chosen in order to monitor the film in the spectral area of its relative transparency, i.e. after the material bandgap (~680 nm). This area is known as Urbach Tail and is characterized by low material absorption (mainly due to the presence of dopants, contaminants and lattice defects) in the vicinity of the conductive zone. Therefore, reasonably high absorption coefficient can be expected at 850 nm. The detection of the film absorption is a feature, which is critical for the determination of the film material bandgap.

In our significant experience in monitoring numerous thin films during deposition, and specifically during this project, the index of refraction and extinction coefficient changes during deposition because of process drift and because of the change in the optical constants of the growing film.

This change, even not sufficiently thought out by most of the thin film solar manufacturers, is very natural and easily explainable. The film growth conditions are different immediately when the film starts growing and forms the interface with the already deposited previous film (or bare substrate), versus the conditions when the film is already thick enough to "forget" its initial growth conditions. Usually at the initial stage of growth the film tends to repeat the morphology of the surface on which it is growing. Therefore, intermixed layers are formed at the interface, which can be structurally and even chemically different than the remaining parts of the film, deposited afterwards. As the film keeps growing the adatoms deposited from the gas phase on the surface start meeting the already deposited particles only of their own material, at which time the growth conditions are changing significantly. As new particles are coming, they trend to shadow each other and stick to areas of the film where the surface energy is larger. The result is the formation of columnar structures and textures with a significant amount of voids and even pores. Thus, the thin film refractive index starts dropping as the film is growing, as predicted by Maxwell—Garnet theory of mixed substances (in this case the mixture of film material with index of refraction of ~4.0 and voids with index of 1.0). This is a phenomenon that is widely observed in most dielectric and semiconductor thin films, and the case of amorphous silicon, which we monitored during this project, is not an exception. Obviously, in our case the large difference between the index of the material and the voids results in more clearly observable change.

This makes the maximums and minimums of the monitored reflectance function during the film deposition, to have reduced amplitude than the previous ones (Figure 9). By continuously monitoring film growth and constantly recalculating the optical constants we found the exact values of the film thickness, refraction and extinction coefficients in different moments of deposition, or at different depths of the film. The constant recalculation process takes place multiple times as reflectance is changing using our iterative prediction capability feature, explained later in this report. For this we use our proprietary calculation algorithm and software which are not a part of this project and are explained elsewhere[3]. Figure 9 shows the change in reflectance and change in the maxima and minima as the film is deposited.

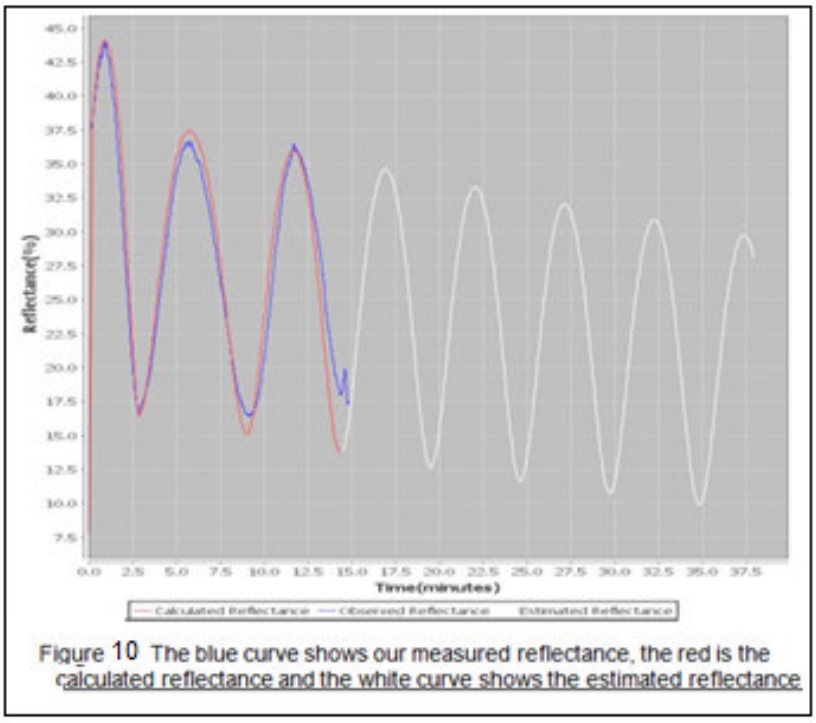

Figure 10 The blue curve shows our measured reflectance, the red is the calculated reflectance and the white curve shows the estimated reflectance

In order to calculate band gap, we have to know the index of refraction and extinction coefficient at different wavelengths. The assumption behind this approach was that once we have calculated the optical constants at 850 nm, we can predict them at different wavelengths. For example, let's say the index of refraction dropped by 10% at 850nm then it would drop by ~10% at all other neighboring wavelengths, including the ones that are in the Urbach zone (where the film bandgap is). Once a prediction is made that the index of refraction has dropped by 10% at, for example, 920 nm, our software recovers the monitored reflectance curve at 920 nm and validates or corrects the index drop. Once the drop is validated and confirmed, then the change is applied to the spectral region of the film material bandgap. The change of the extinction coefficient at 850 nm is likewise applied to the Urbach zone and therefore, a change in the material bandgap is calculated.

Figure 10 shows the change in the optical constants as the film grows. Using this information, we used the Cody's and Tauc's formulae[4],[5] to calculate the material bandgap:

$$\alpha / E = [B_0(E - E_g)]^2 - \text{Cody}$$

$$\alpha . E = [C_0(E - E_g)]^2 - \text{Tauc}$$

where α is absorption coefficient (cm^{-1}), E is energy (eV), E_g is the bandgap energy of the film material (eV), n is the film refractive index and B_0 and C_0 are constants.

[3] G. Atanasoff, OSA Technical Digest, Optical Interference Coatings Topical Meeting, Tucson, AZ, June 6-11 (2010);
[4] G.D. Cody et al., *Sol. Energy Mater.*, **8**, 231-238 (1982);
[5] A.M. Bakry and A.H.El-Naggar, *Thin Solid Films,* **360** 293-297 (2000);

In order to calculate band gap we need to plot $(\alpha/E)^{1/2}$ or $(\alpha.E)^{1/2}$ against energy. The intersection of the extrapolation of the linear region in the Cody's and or Tauc's plots with x-axis gives the bandgap energy. This is shown in Figure 11 for the case of Cody's plot.

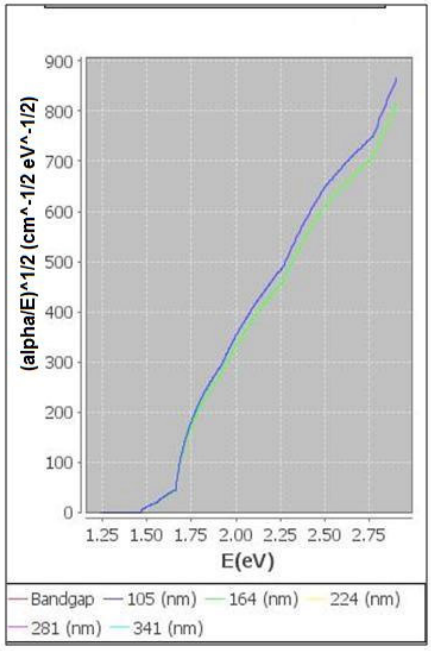

Figure 11. Bandgap as a function of energy for two different film thicknesses.

Problem: The problem with using the intersection of the extrapolated portion of the curve with the x-axis was that we kept on getting the same band gap value even though the optical constants change. The reason is in the assumption that the change in the optical constants is uniform across all the wavelengths. Therefore, the wavelength at which α=0 will always be the same (since 0*10% = 0). This approach only tilts the plot, but the intersection with α=0 remains unchanged, resulting in the determination of the same value for the bandgap. In reality the absorption coefficient curve may not only tilt, but may also shift versus its spectrums, and the bandgap change is associated with the shift, rather than with the tilt. Figure 11 shows that though the Tauc's plot has changed, the band gap (X-Intercept) value is same for both curves.

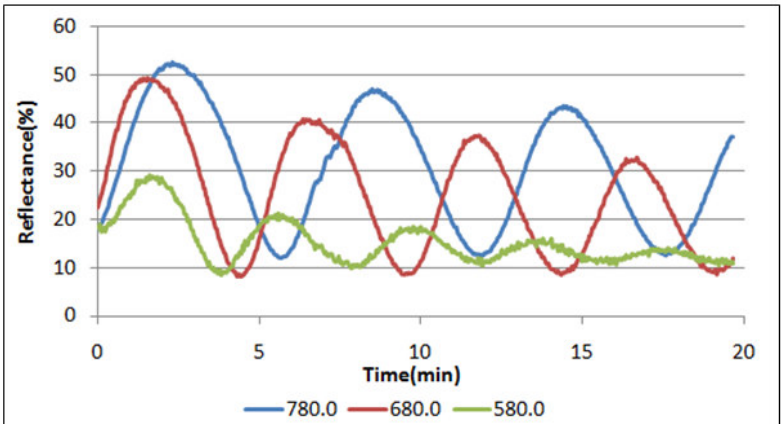

Figure 12. Reflectance as a function time at three wavelengths, 580, 680 and 780nm.

Solution: Monitoring at one wavelength is not enough to calculate the bandgap and, therefore we chose to monitor at multiple wavelengths. We made use of a spectrometer which has the ability of monitoring reflectance from 400 nm to 950 nm. We did all the calculations of optical constants that we did in approach 1, but this time we repeated them for the following wavelengths: 580, 600, 640, 660, 680, 700, 720, 740, 760, 780, 800, 820, 860, and 920. These wavelengths were chosen so as to have monitoring in the high absorption (580, 600, and 640), medium absorption (660, 680, 700, 720, 740, 760, and 780) and low absorption (800, 820, 860, and 920) regions of amorphous silicon. Since the optical properties for amorphous silicon are different at different wavelengths, the monitored reflectance functions are also different. This is illustrated in Figure12. As can be seen, as higher wavelengths have less absorption

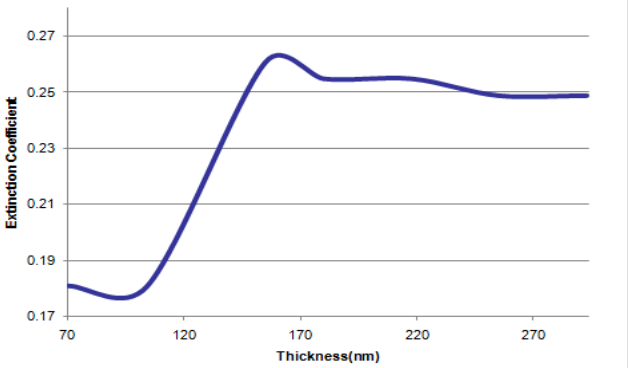

Figure 13. Extinction coefficient as a function of film thickness as calculated from the reflectance.

and more reflectance. Also the turning points are wider and happen at later times compared to lower wavelengths. These observations are important for calculating the optical constants at different wavelengths. Extinction coefficients at all the wavelengths are calculated. Figure 13 shows the extinction coefficient as a function of film thickness calculated for 680 nm. The calculation of k at all wavelengths leads us to Tauc's plot and to the calculation of the bandgap of the amorphous silicon.

In order to test the validity of this method, we calculated the band gap and extinction coefficient on bench top using transmittance and reflectance measurement. Using these, absorption coefficient could be calculated as follows:

$$\alpha = \frac{-1}{d} \ln\left[\frac{T}{(1-R)^2}\right]$$

Where, α is the absorption coefficient (cm^{-1}), T is the transmittance, R is the reflectance, d is the thickness of the film (nm).

Using this calculated absorption coefficient, we calculated

1. Tauc plot to find out band gap.
2. k, extinction coefficient.

The result shows that band gap calculated on bench top using Transmittance and Reflectance measurements and the one calculated in real time as the film is growing are very close. As can be seen from Figure 14 and 15 the band gap value using real time measurement is 1.60 and the one using bench top system is 1.62.

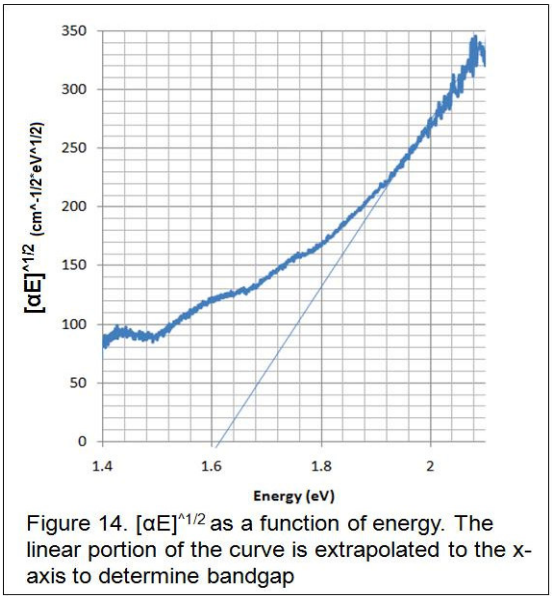

Figure 14. $[\alpha E]^{\wedge 1/2}$ as a function of energy. The linear portion of the curve is extrapolated to the x-axis to determine bandgap

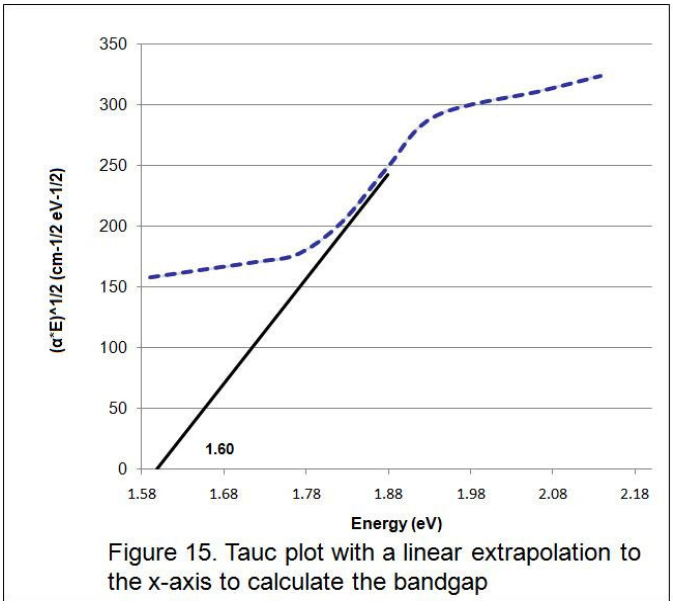

Figure 15. Tauc plot with a linear extrapolation to the x-axis to calculate the bandgap

In order to prove the validity of our bench top system, we calculated the extinction coefficient from the absorption coefficient measurement. The graph shows that k values calculated using the bench top system are very close to the standard values which are also close to our in situ measurements.

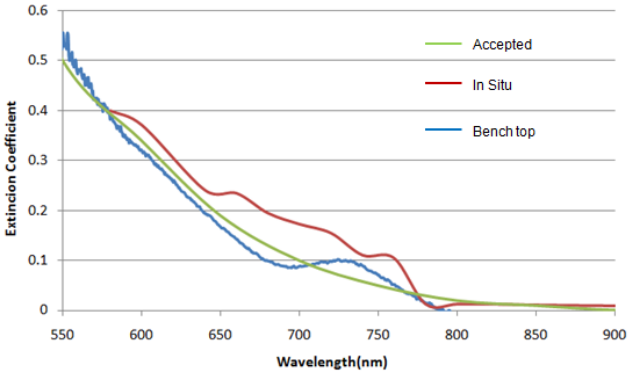

Figure 16. Extinction coefficient comparison of the accepted values, as measured *in situ* and calculated from the transmission and reflectance measurements in a bench top environment.

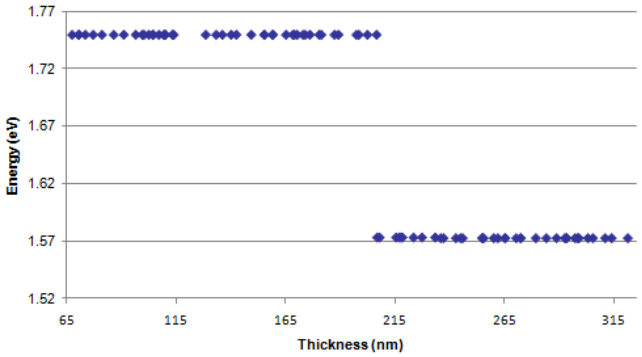

Figure 17. The bandgap is calculated from the reflectance as the thickness of the film increases. The bandgap in this figure changes at a thickness of about 205nm.

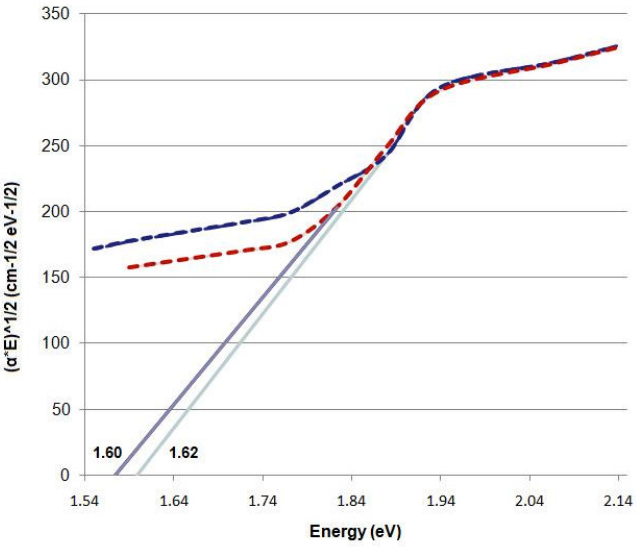

Figure 18. The Tauc calculation is shown for two bandgap measurements. The linear region of the plot is extrapolated to the x-axis to determine the bandgap energy

Results:

The obtained results significantly support our view of monitoring band gap in real time. The band gap not only varies from one deposition to the next but it also varies within one deposition. This happens because the optical properties of the material are highly dependent on process parameters which drift with time. Figure 16 shows the variation in extinction coefficient at 640nm as the film grows. These variations of optical parameters change the band gap value of amorphous silicon from its standard value of 1.75 as shown in Figure 17. The band gap does not only vary from its standard value but it also varies panel to panel. Figure 18 shows how the band gap differs for two panels deposited at same time.

Subtask 3.3 Develop an iterative prediction algorithm for the two sensor arrays

The iterative prediction algorithm is one of the main software features developed by AccuStrata since 2007. The iterative prediction capability for the determination of the material bandgap was developed under this project.

The concept of the iterative prediction capability is based on monitoring the film deposition in real time and the software calculates the required parameters multiple times per second. The concept can be explained by the following sequence of events that are performed by the software program:

1. Monitor the reflectance function as the film is being deposited
2. Based on one concrete measurement in time calculate the required parameter (in this case the material bandgap)
3. Based on the calculated value predict how the reflectance

function will behave next
4. If the monitored function behaves as predicted, validate the calculated value
5. If the monitored function does not behave as predicted, recalculate a new parameter value and make a new prediction
6. Repeat the process until there is a match between the real monitored function and the predicted one
7. Operations 1-6 transpire during the entire monitoring cycle

This capability, built on our monitoring and control system operation software allows us to achieve much higher parameter calculation accuracy than would be achieved if the calculation is made based only on measurements taken during a single point in time.

During this DoE Supply Chain project our activity was focused on developing this capability not only in time, but also from the two separate fiber optics sensors.

The software program was made to constantly search the results of the calculations for both sensors and compare them to each another. Since the calculation of the material bandgap is a subjective process, the calculations for the two sensors have to be compared in real time in order to obtain similar and realistic values.

The way this was implemented in our software was described in the previous section, when we explain the bandgap determination procedure from the calculation of the absorption coefficient at multiple wavelengths. One static graphical representation of the iterative prediction capability is also shown in Figure 19 in the next section, when the validation of the system is described. In Figure 19 one can see how the measured signal is changing, how our software calculation matches the measured signal and how the future behavior of the monitored signal is predicted based on the parameter calculations at the moment.

However, better graphical representation of the iterative prediction capability built during this project can be given in a video demonstration when the entire process is played in time. For more details one can go to our website video demonstration at www.accustrata.com/demonstration.

Problem: One has to take into account the fact that material bandgap is a well-defined parameter only for ideal crystalline substances at low temperatures. In reality all practical materials have fussy boundaries of the conductive and valence zones, populated with multiple energy levels due to contaminants, dopants, defects and other carrier traps. This is especially true for thin films, which grow at far from thermal equilibrium conditions. Therefore, in most cases the absolute value of the material bandgap has a more scholastic than a practical value.

Solution: The experience we gained throughout this project shows that the manufacturer are not interested in the absolute value of the bandgap, but are interested mainly in whether the material bandgap **changes** during the deposition and over the area of the panel. This makes our task easier. We created a procedure (convention) how to determine the bandgap value and implemented it each time in the same way. This allowed us to find whether the bandgap changes during the deposition and from one area to another, without being too much fixated on the absolute value.

As a result Task 3 has been completed 100%. The milestone has been achieved

Task 4: Validate the system in real thin film solar panel deposition process

Approach:
Under this task, we installed our fiber optic sensors in the pilot line at Sencera International, in Charlotte, NC. The sensors were installed on the back side of the substrate so as to prevent them from getting coated. We use a halogen bulb coupled into 600 μm fiber as an illumination source and collect the reflected data using an optical fiber connected to the spectrometer. A software program controlled the spectrometer to make a scan at a particular rate in time. The data acquisition component collects this data from the spectrometer and makes a data packet. This data packet is then sent to the analysis component of the software and also saved to a file for future reference. The analysis component performs the following tasks:

1. Gives visual representation of the measured data.
2. Calculates the optical properties of the film.
3. Iteratively predicts the behavior of the reflectance signal in future time.
4. Incrementally corrects the calculations as more and more data is collected.

Problems and Solutions:
Most of the problems with the real time measurement of thin film growth are already discussed in the previous sections.

Results:

Figure 19 shows the reflectance measurement at 680nm. As the measured signal goes through maxima and minima, the analysis software synchronizes the calculated signal by changing the optical constants. The figure shows the match between measured and calculated signal. Using these optical constants and assuming that they do not change, software predicts the behavior of the reflectance signal. As can be seen, the red line follows the blue line meaning the predictions are close to correct.

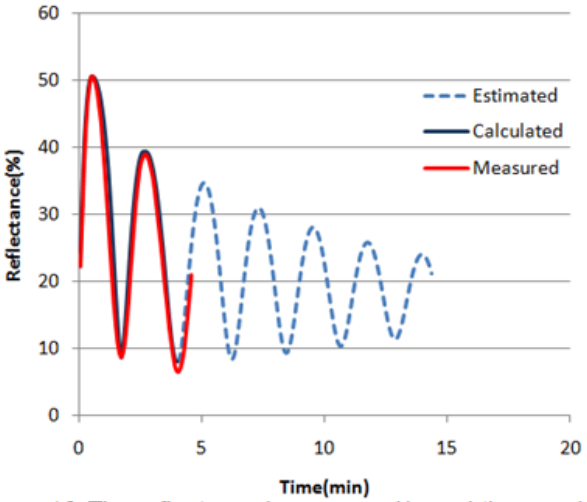

Figure 19. The reflectance is measured in real-time, and the algorithm predicts how the reflectance will change with the thickness of the film and corrects any error in previous estimates. This algorithm updates at the turning points (local maxima and minima).

Using the reflectance measurements, we calculate in real time,

1. Thickness of the film (shown in Figure 20)
2. Rate of deposition
3. Uniformity across the panel
4. Band gap of the absorber
5. Surface roughness

We installed two fiber optic sensors to monitor two different locations on the panel. This makes

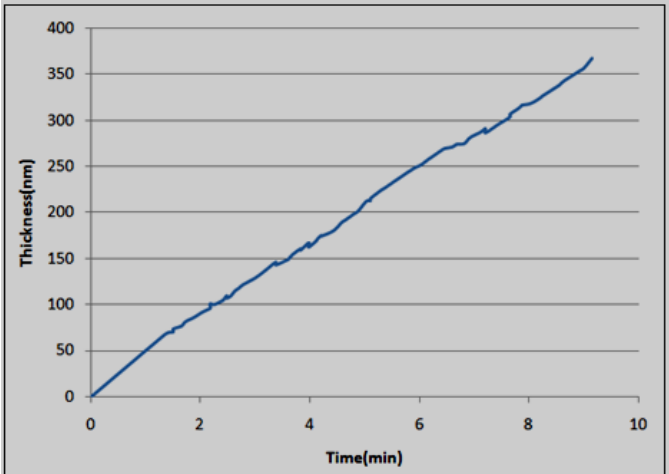

Figure 20. Thickness at one location is shown. The deposition rate is fairly constant

sure that the film growth is uniform over the area of the panel. All calculations are performed at two different locations on the panel which gives a correct measure of uniformity across the panel.

Figure 21 shows the variation in the thickness growth at two different regions of the panel. Any non-uniformity is displayed on screen with a differential curve. The non-uniformity in film growth can also be seen in the reflectance signal as shown in Figure 22.

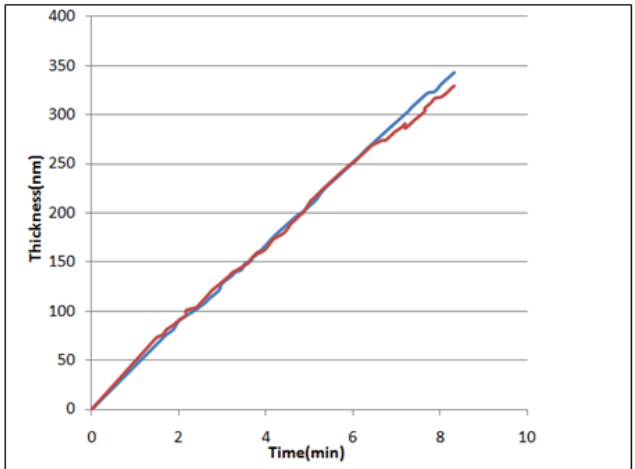

Figure 21. Thickness is measured at two separate locations of the same substrate under deposition. The deposition rate begins to differ and the thickness therefore begins to deviate

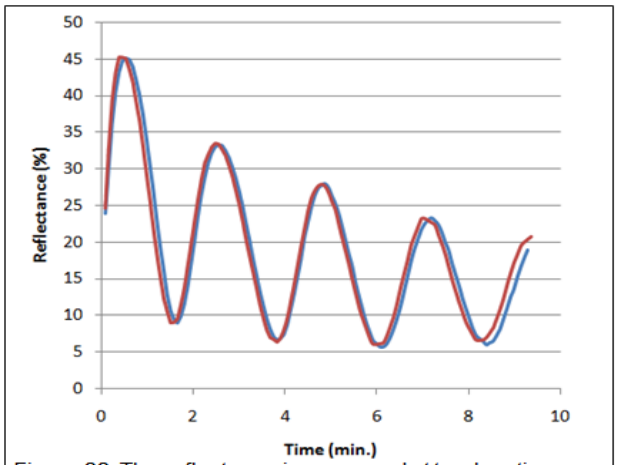

Figure 22. The reflectance is measured at two locations on the substrate as the deposition occurs. The deviation in thickness can be seen here where the reflectance curves begin to differ.

Products developed under the award

Publications:

1. George Atanasoff and Oscar von Bredow, Intelligent Optical Control for the Manufacturing of More Efficient Thin Film Solar Panels, *Energetica India*, issue Nov/Dec 2009, pg. 34-36;
2. George Atanasoff, Real Time Optical Monitoring of Properties of Silicon Thin Film Solar Panels, OSA Technical Digest, OIC Topical Meeting, Tucson, AZ, June 6-11, 2010;
3. George Atanasoff, George Atanasoff, Real Time Optical Monitoring of Properties of Silicon Thin Film Solar Panels, OSA Technical Digest, Congress in Optics, SOLAR, Tucson, AZ, June 7-10, 2010;

Computer Modeling Results

All computer modeling that was performed under this project have been described in the above sections.